Biaxial order in liquid crystals and their mixtures: A Potts-Ising model

Robert G. Caflisch,* Zhong-Ying Chen,† and A. Nihat Berker
Department of Physics, Massachusetts Institute of Technology, Cambridge, Massachusetts 02139

John M. Deutch
Department of Chemistry, Massachusetts Institute of Technology, Cambridge, Massachusetts 02139
(Received 20 June 1984)

A lattice model for binary mixtures of prolate and oblate molecules is studied, by a mapping onto a 13-state Potts-Ising model, followed by an approximate renormalization-group analysis. Four different types of phase diagram are obtained, exhibiting prolate uniaxial, biaxial, and oblate uniaxial phases. Local disorder has the nonordering property of an effective vacancy and is thus included into our mapping. Such effective vacancies can cause first-order phase transitions. Thus the biaxial phase can disorder either directly through a ridge of first-order transitions, or via an intermediate uniaxial phase which vanishes at a multicritical point. In the biaxial region, the system is shown to be related to the six-state clock model, so that the latter point may be replaced by a segment of algebraic (Kosterlitz-Thouless) order in films. Similar considerations are applied to one-component systems of biaxially shaped molecules.

I. INTRODUCTION

The preferential orientation of the microscopic constituents of a system along two orthogonal directions is a subject of both experimental and theoretical interest. Such a possibility, within the context of liquid-crystal systems, was studied some time ago by Alben and others.[1–4] More recently, experimental realization was achieved in the amphiphilic systems composed of potassium laurate or sodium decylsulfate, decanol, and water.[5] The delicate equilibrium involved in such a phase is apparent from qualitative microscopic considerations: For a system of identically shaped molecules, preferential orientation along one direction results in energy stability and delegates entropy gains to fluctuations in the transverse directions, thus hindering the possibility of alignment along any of the latter. For systems of multishaped molecules, the orientational order of one species requires a network of the corresponding molecules which not only percolates, but also maintains a strong connectivity. For a second species to order, a similar network is required, with the added spatial hindrance that each network would have to permeate the other.

We have studied biaxial ordering by generalizations of the lattice model for uniaxial ordering introduced by Zwanzig.[6] In Zwanzig's model, a single species of molecules with one distinguishable axis lies at the sites of a cubic lattice. Each molecular axis can align along one of the three lattice axes. The intermolecular interactions induce uniaxial order. In Sec. II we present a generalization which includes two uniaxial species, prolate and oblate particles. The lattice model for the binary mixture of prolate and oblate molecules is prefaced[7,8] onto a 13-state Potts-Ising model. This model, in turn, is subjected to the renormalization-group analysis of a Migdal-Kadanoff procedure.[9,7] The renormalization-group flows of 21 different interaction constants are included in the analysis. Although these prefacing and renormalization procedures involve uncontrolled approximations, they can be expected, on phenomenological grounds, to provide qualitative indications of the true system behavior (Sec. III). Another generalization, involving a single species of biaxially shaped molecules, maps onto a subspace of our Potts-Ising model and yields similar phase diagrams (Sec. V).

Our study also illustrates the role of effective vacancies,[10] namely, regions of local disorder which, by condensing, precipitate a first-order phase transition with latent heat. Depending on the preponderance of such effective vacancy regions, one of four types of phase diagram is found to occur (Sec. III). These are distinguished by (i) no biaxial phase, (ii) a biaxial phase which, upon increasing temperature, disorders across a ridge of first-order transitions, (iii) and (iv) a biaxial phase which disorders via an intermediate uniaxial phase, except for a direct disordering through a single multicritical point or a segment of algebraic order.[11] In connection with the latter, we show that the biaxial degrees of freedom of this lattice model reproduce a six-state clock model.[12] Thus, in two dimensions, the model should exhibit a temperature range of algebraic biaxial order (Sec. IV). The first-order transitions disordering the uniaxial phases are characterized by very narrow coexistence regions and small latent heats, as is observed experimentally with nematic liquid-crystal transitions.[1,2]

II. THE LATTICE MODEL AND ITS TREATMENT

A. The lattice model

We begin with the case of binary mixtures, since it leads to the most general Potts-Ising model that we have considered. The starting lattice model is a straightforward generalization of the one presented by Zwanzig:[6] Each site of a hypercubic lattice is occupied by a uniaxially shaped molecule which is either prolate (referred to as a rod) or oblate (plate). The axis of each molecule so

TABLE I. Interaction energies between nearest-neighbor cells in configurations C_1 and C_2.

C_1	C_2					
	Z	X	$\bar{Z}$	$\bar{X}$	$Z\bar{X}$	$X\bar{Y}$
Z	0	$4J_R$	$4J_X$	0	0	$2J_R$
$X\bar{Z}$	$2J_R+2J_X$	0	0	$2J_X+2J_P$	$J_R+2J_X+J_P$	J_P

described aligns with one of three lattice axes. Overlap of neighboring molecules is energetically disfavored, so that the nearest-neighbor interaction energy depends on the molecular alignments, differently, of course, for rod-rod, rod-plate, and plate-plate pairs.

Let the variables $s_i=x,y,z$ or $\bar{s}_i=\bar{x},\bar{y},\bar{z}$ denote the occupation of site i by a rod (unbarred) or a plate (barred) aligned with each of the lattice axes. Then a simple Hamiltonian for the system is

$$\mathcal{H}=\sum_{\langle ij\rangle}\{J_R t_i t_j[f_R-\delta(s_i,s_j)] +J_X[t_i\bar{t}_j\delta(s_i,\bar{s}_j)+\bar{t}_i t_j\delta(\bar{s}_i,s_j)] +J_P\bar{t}_i\bar{t}_j[f_P-\delta(\bar{s}_i,\bar{s}_j)]\}+\mu\sum_i(t_i-\bar{t}_i)\,, \tag{1}$$

where $(t_i,\bar{t}_i)=(1,0)$ or $(0,1)$ for rod or plate occupation of site i, δ equals 1 (0) if its arguments refer to the same (different) lattice axis, $\langle ij\rangle$ denotes summation over nearest-neighbor[13] pairs of sites, and the coupling constants J_α are non-negative. The final term introduces the chemical potential difference which controls the rod and plate concentrations. The above Hamiltonian involves a simplifying approximation in that the interaction energy of a pair of molecules has been averaged over the six possible lattice directions between such nearest-neighbor molecules, which is reasonable for modeling a liquid system. As Eq. (1) is now, the first and third terms are ferromagnetic Potts[14] couplings, while the second term is an antiferromagnetic Potts coupling.[15] We shall report here results for $f_R=f_P=1$, applicable to systems in which favorably aligned pairs have essentially equivalent interaction energies, irrespective of the constituent species.

B. Prefacing transformation

In a renormalization-group treatment of this microscopic model, the first few rescaling transformations could be of considerable importance to yield biaxial order. This is because these rescalings would generate further-neighbor interactions which could maintain the connectivity of two interpenetrating, orthogonally oriented networks, as mentioned above. On the other hand, renormalization-group transformations that directly include further-neighbor interactions are cumbersome. This technical difficulty can be avoided by considering the nearest-neighbor interaction between small regions of the system, thereby, in effect, including further-neighbor interactions of the molecular level.[7,8]

The small regions that we use are $2\times2\times2$ cells, and can reflect the following local properties: aligned rod (X, Y, or Z), aligned plate ($\bar{X}$, $\bar{Y}$, or $\bar{Z}$), biaxially aligned ($X\bar{Y}$, $X\bar{Z}$, $Y\bar{Z}$, $Y\bar{X}$, $Z\bar{X}$, or $Z\bar{Y}$), or disordered (0). The latter is the effective vacancy state. The cell Hamiltonian should in principle be determined by partially summing all of the partition function, over the molecular degrees of freedom consistent with fixed cell states. This is done here in a simple approximation. The chemical potential for each of the above cell states ($C=X,Y,Z,\bar{X},\ldots$) is obtained from a single-cell summation:

$$e^{-\beta\mu_C}=\sum_{\{t,\bar{t},s,\bar{s}\}}^{2\times2\times2}e^{-\beta\mathcal{H}_C}\,, \tag{2}$$

where $\mathcal{H}_C$ is the part of the molecular Hamiltonian which is contained in one cell. For the aligned-rod cell state, for example $C=Z$, the sum includes all molecular configurations with at least six rods aligned with the z axis. The corresponding requirement of at least six aligned plates is used in obtaining the chemical potential of an aligned-plate cell state. For the biaxially aligned cell state, such as $C=Z\bar{X}$, the single-cell sum includes all molecular configurations with at least three rods and three plates aligned respectively with the z and x axes. Finally, the effective-vacancy cell state is assigned all molecular configurations of the cell which are not assigned to the uniaxially or biaxially aligned cell states.

To proceed with the analysis, the right side of Eq. (1) must be converted into a polynomial in the four variables $e^{\beta J_\alpha}$ and $e^{\beta\mu}$, so that this prefacing transformation can be effected for any given molecular parameters. However, even with our single-cell approximation, this leads to very long polynomials, causing computer storage and computing time difficulties. Thus, as a further approximation, the Boltzmann average

$$J=\frac{J_R e^{-\beta(J_R+2\mu)}+2J_X e^{-\beta J_X}+J_P e^{-\beta(J_P-2\mu)}}{e^{-\beta(J_R+2\mu)}+2e^{-\beta J_X}+e^{-\beta(J_P-2\mu)}} \tag{3}$$

is used for all the intracell molecular energies. The resulting polynomials, in the two variables $e^{\beta J}$ and $e^{\beta\mu}$, manageably contain 1899 terms.

The intercell energies are estimated even more simply. An effective-vacancy cell has zero interaction with any neighboring cell. An aligned cell is pictured as composed of two labels, e.g., $ZZ\equiv Z$ or $\bar{Z}\,\bar{Z}\equiv\bar{Z}$ for uniaxially and $Z\bar{X}$ for biaxially aligned cells. Two nearest-neighbor cells interact via the interaction constants and δ functions of Eq. (1), with the cell labels as arguments (Table I). Note

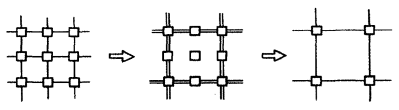

FIG. 1. Migdal-Kadanoff renormalization procedure. In the first, approximate, step, some of the bonds are moved. In the second step, intermediate degrees of freedom are summed over.

TABLE II. Exponentiated cell Hamiltonian $w(C_1,C_2)=\exp[-\beta\mathcal{H}(C_1,C_2)]$ per nearest-neighbor pair of cells.

C_1 \ C_2	0	X	Y	Z	$X\bar{Y}$	$X\bar{Z}$	$Y\bar{Z}$	$Y\bar{X}$	$Z\bar{X}$	$Z\bar{Y}$	$\bar{X}$	$\bar{Y}$	$\bar{Z}$
0	w_1	w_{11}	w_{11}	w_{11}	w_{12}	w_{12}	w_{12}	w_{12}	w_{12}	w_{12}	w_{13}	w_{13}	w_{13}
X	w_{11}	w_2	w_3	w_3	w_{14}	w_{14}	w_{15}	w_{16}	w_{16}	w_{15}	w_{17}	w_{18}	w_{18}
Y	w_{11}	w_3	w_2	w_3	w_{16}	w_{15}	w_{14}	w_{14}	w_{15}	w_{16}	w_{18}	w_{17}	w_{18}
Z	w_{11}	w_3	w_3	w_2	w_{15}	w_{16}	w_{16}	w_{15}	w_{14}	w_{14}	w_{18}	w_{18}	w_{17}
$X\bar{Y}$	w_{12}	w_{14}	w_{16}	w_{15}	w_4	w_5	w_6	w_7	w_6	w_8	w_{19}	w_{21}	w_{20}
$X\bar{Z}$	w_{12}	w_{14}	w_{15}	w_{16}	w_5	w_4	w_8	w_6	w_7	w_6	w_{19}	w_{20}	w_{21}
$Y\bar{Z}$	w_{12}	w_{15}	w_{14}	w_{16}	w_6	w_8	w_4	w_5	w_6	w_7	w_{20}	w_{19}	w_{21}
$Y\bar{X}$	w_{12}	w_{16}	w_{14}	w_{15}	w_7	w_6	w_5	w_4	w_8	w_6	w_{21}	w_{19}	w_{20}
$Z\bar{X}$	w_{12}	w_{16}	w_{15}	w_{14}	w_6	w_7	w_6	w_8	w_4	w_5	w_{21}	w_{20}	w_{19}
$Z\bar{Y}$	w_{12}	w_{15}	w_{16}	w_{14}	w_8	w_6	w_7	w_6	w_5	w_4	w_{20}	w_{21}	w_{19}
$\bar{X}$	w_{13}	w_{17}	w_{18}	w_{18}	w_{19}	w_{19}	w_{20}	w_{21}	w_{21}	w_{20}	w_9	w_{10}	w_{10}
$\bar{Y}$	w_{13}	w_{18}	w_{17}	w_{18}	w_{21}	w_{20}	w_{19}	w_{19}	w_{20}	w_{21}	w_{10}	w_9	w_{10}
$\bar{Z}$	w_{13}	w_{18}	w_{18}	w_{17}	w_{20}	w_{21}	w_{21}	w_{20}	w_{19}	w_{19}	w_{10}	w_{10}	w_9

that this provides four intercellular bonds for a pair of cells, as in the original molecular model.

C. Renormalization-group transformation

The renormalization-group transformation, in the Migdal-Kadanoff approximation,[9,7] is effected by moving bonds and summing over the states of a subset of the cells (Fig. 1). The corresponding algebraic statement is[8]

$$w'(C_1,C_2)=\sum_C [w(C_1,C)w(C,C_2)]^2 , \tag{4}$$

where

$$w(C_1,C_2)=e^{-\beta\mathcal{H}(C_1,C_2)}$$

is the exponentiated cell Hamiltonian per nearest-neighbor pair of cells. The sum is over the 13 states of the intermediate cell. The symmetry of $w(C_1,C_2)$ as it recurs under the renormalization group is given in Table II, where the 1×1 effective-vacancy, 3×3 rod-uniaxial, 6×6 biaxial, and 3×3 plate-uniaxial block structure is delineated. The rod-rod, plate-plate, and rod-plate blocks show ferromagnetic and antiferromagnetic Potts couplings, respectively. The effective-vacancy block introduces an Ising degree of freedom. The biaxial block shows the couplings of a clock model, to be discussed in Sec. IV below. The phase diagrams are deduced by globally tracing the renormalization-group flows, in the 21 distinct coupling constants exponentiated in Table II, to the fixed points.[16,7,8] We have effected the Migdal-Kadanoff transformation here in $d=2$ spatial dimensionality, which enters only the bond-moving step. It is known that the Migdal-Kadanoff approximation overrepresents spatial dimensionality.[17,18] Thus, for our present purposes, a $d=2$ calculation should give qualitative indications for the three-dimensional behavior.

III. PHASE DIAGRAMS FOR MIXTURES OF PROLATE AND OBLATE MOLECULES

The phase diagram, calculated as described above, is shown in Figs. 2(a) and 2(b) in the spaces of temperature versus chemical potential and density, respectively. As representative values, $J_X=0.75J_R$ and $J_P=0.5J_R$ have been adopted. Prolate and oblate uniaxially ordered phases occur, respectively, in regions of high rod and plate concentrations. They are separated from the isotropic (disordered) phase by first-order boundaries. These first-order transitions are characterized by extremely narrow coexistence regions and small latent heats, as is observed experimentally with nematic liquid-crystal transitions.[1,2] At this stage, no biaxial phase is seen and the isotropic phase extends to zero temperature at intermediate concentrations.

Previous work,[17] on the other hand, has shown that the Migdal-Kadanoff procedure may overestimate the role of effective vacancies. We have investigated calculations with such a role diminished, by artificially adding, after the prefacing transformation, a chemical potential μ_A to the effective-vacancy cell state. The inclusion of such an adjustable parameter may be viewed either as exploring possibilities admitted by the indeterminacy of an uncontrolled approximation, or as taking into account the close-packed character of realistic systems (repressing effective vacancies in contrast to the open-packed cubic lattice), or as mimicking a metastable system which is superheated past the first-order transitions.

As the effective vacancies are repressed by making μ_A more negative, the first-order transitions recede to higher temperatures. A biaxially ordered phase appears at comparable rod and plate concentrations [Figs. 2(c) and 2(d)]. It is flanked by prolate and oblate uniaxially ordered phases. The transitions between the biaxial phase and uniaxial phases of this model are second order and governed by a fixed point of Ising criticality. All three

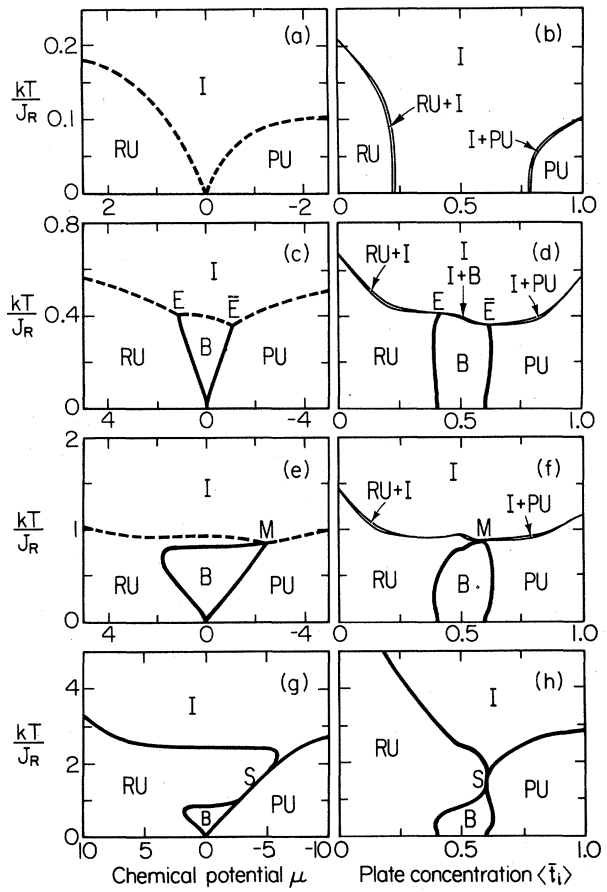

FIG. 2. Calculated phase diagrams for rod-plate mixtures with $J_X=0.75J_R$ and $J_P=0.50J_R$. In (a),(b); (c),(d); (e),(f); and (g),(h), $\mu_A=0$; $-8J_R$; $-20.8J_R$; and $-\infty$, respectively. The rod-uniaxial, biaxial, plate-uniaxial, and isotropic phases are labeled RU, B, PU, and I, respectively. The arrows point to the coexistence regions, which are very narrow. Second-order boundaries are indicated by the thick solid lines, while first-order transitions are indicated by the dashed lines and by the thin lines around the coexistence regions. The critical endpoints (E and $\bar{E}$), the multicritical point (M), and the six-state clock multicritical point (S) are noted.

ordered phases disorder by first-order transition, again characterized by narrow coexistence regions and small latent heats. This is a new phase-diagram topology, also independently discovered in a Landau theory study[4] which was communicated to us after this work was completed. The isotropic, uniaxial, and biaxial phases meet at critical endpoints (E and $\bar{E}$). As a technical curiosity it may be noted that each uniaxial phase is realized, under renormalization group, in two ways. For example, the rod-aligned phase with the z axis is realized, to the left of the phase diagrams, by the dominance of the Z cell state. More to the center of the diagrams, this phase is realized by the intermingled dominances of $Z\bar{X}$ and $Z\bar{Y}$. The two basins are separated by a renormalization-group null line,[8] controlled by an Ising infinite-temperature fixed point.

Figures 2(e) and 2(f) show $\mu_A=-20.8J_R$, for which value the two critical endpoints merge. The two critical

TABLE III. Multicritical fixed points. For both fixed points, all x_n^* that are not shown vanish. All y_n that are not shown are irrelevant (negative).

(a) M^*

Location ($x_n \equiv w_n/w_4$)

$(x_1;x_5=x_8,x_6,x_7;x_{12})^*=(0.775;0.484,0.202,0.146;0.557)$

Relevant eigenvalue exponents:

$(y_1,y_2,y_3)=(1.444,0.619,0.533)$

(b) S^* (six-state clock)

Location

$(x_5=x_8,x_6,x_7)^*=(0.685,0.235,0.080)$

Relevant eigenvalue exponents:

$(y_1,y_2)=(0.840,0.167)$

lines meet on the first-order boundary at point M. Under renormalization group, this point is controlled by its own fixed point M^* [Table III(a)] in the full space of the flows. Thus the point M has its own distinctive scaling exponents, three of which are relevant [y_{1-3} in Table III(a)]. This leads us to conclude that M is a novel multicritical point. The four phases thus meet at M, where there is a direct, higher-order transition between the biaxial and isotropic phases. On each side of M, the disordering lines of the uniaxial phases are still weakly first order. This phase diagram topology was previously obtained by mean-field studies[1-3] and is hereby confirmed by renormalization group. It is consistent with the experimental results to date.[5]

For more negative values of μ_A, second-order segments (of three-state Potts criticality) emanate from the four-phase point onto the disordering boundaries. Such segments, also emanating from the two pure-system limits, are bounded by tricritical points. The four-phase point [S in Figs. 2(g) and 2(h)] becomes the confluence of four second-order boundaries and changes multicritical character. Its governing fixed point S^* is given in Table III(b). This multicritical point is more stable than M. It corresponds to the six-state clock transition, which is again direct between the biaxial and isotropic phases, discussed in Sec. IV below. Figures 2(g) and 2(h) show the case of $\mu_A=-\infty$, which totally represses effective vacancies and the concomitant first-order transitions. This topology, modified for algebraic order in the neighborhood of S, is an interesting candidate for the behavior of experimental thick films (see below). By contrast, the multicritical topology of Figs. 2(e) and 2(f) may be associated with bulk behavior.

IV. SIX-STATE CLOCK BEHAVIOR

In order to further understand the multicritical point S, first consider the case of $J_R=J_X=J_P\equiv J$. The phase diagram is then symmetric and the multi-critical point S occurs on the symmetry line of $\mu=0$ and of equal road and plate concentrations. On this line, the biaxial cells are dominant at low temperature. Consider such a cell in the $Z\bar{X}$ state. Figure 3(a) shows the interaction energies due to a neighboring cell in the various biaxial states. These

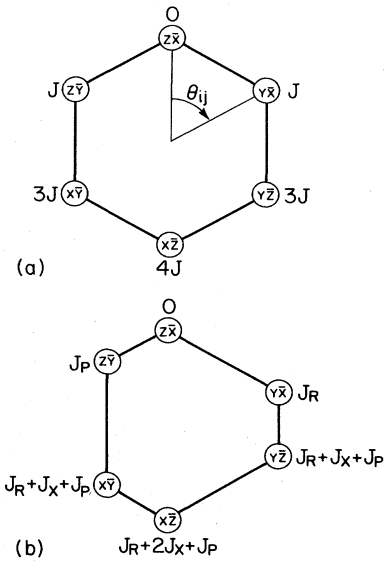

FIG. 3. For a given cell in state $Z\bar{X}$, interaction energies for the various states of a nearest-neighbor cell. (a) The symmetric $J_R=J_X=J_P$ case leads manifestly to the six-state clock model: The interaction is of the form $2J(1-\cos\theta_{ij})$, $\theta_{ij}=\theta_i-\theta_j$, where each cell state C_i defines an angle θ_i which is an integer multiple of $\pi/3$. (b) The asymmetric $J_R\neq J_P$ case gives a "paired" six-state clock model, which, from points of comparable concentrations, unpairs under renormalization. For large concentration differences, under renormalization group, pairwise coalescence of the six states yields the (threefold) uniaxial phases.

are the energy relationships of a six-state clock model.[12]

For $J_R\neq J_P$, the six-state model is "paired," as shown in Fig. 3(b). The multi-critical point S occurs at unequal road and plate concentrations, which appear to compensate the interaction pairing: Under rescaling, the multicritical point renormalizes to an unpaired six-state clock model. Note that we define a general "paired" six-state clock model by

$$J(Z\bar{X},Z\bar{X})<\{J(Z\bar{X},Y\bar{X})\neq J(Z\bar{X},Z\bar{Y})\}$$
$$<J(Z\bar{X},X\bar{Y})=J(Z\bar{X},Y\bar{Z})\leq J(Z\bar{X},X\bar{Z})\ . \quad (5)$$

In all biaxial phases and biaxial-isotropic phase boundaries of the present study, energies renormalize to the general "unpaired" model, defined by modifying Eq. (5) with

$$J(Z\bar{X},Y\bar{X})=J(Z\bar{X},Z\bar{Y})\ . \quad (6)$$

Of novel interest here is the two-dimensional version of the model. This would have to be several layers thick, in order to accommodate two percolating clusters and, thereby, biaxial order. In that case, from the properties of the six-state clock model,[12] and intermediate temperature range of algebraic (Kosterlitz-Thouless[11]) biaxial order would be expected, followed by conventional biaxial order at low temperatures. In fact, the phase diagram could very much look like Figs. 2(g) and 2(h) with the region where the two second-order boundaries stay together being in reality replaced by the segment of algebraic order, distinguished by continuously varying (nonuniversal) critical exponents.

The next question is whether such behavior could emerge in experimental systems, where the three discrete lattice axes are replaced by continuous rotational symmetry. One analogous situation involves the two-dimensional (continuous) XY model. A prefacing transformation which projects the signs of the cosine and sine of the local angle is indeed seen[19] to connect approximately the Kosterlitz-Thouless phase to the nonuniversal critical line of the (discrete) Ashkin-Teller model. Thus this new possibility in the biaxial systems certainly deserves experimental and further theoretical consideration.

V. SYSTEMS OF SINGLE-COMPONENT, BIAXIAL MOLECULES

Consider the lattice model of a single species of biaxial molecules. A molecule is represented by a rectangular prism with edge lengths $a>b>c$. It can orient along the lattice axes, thus being in one of six states labeled, for example, by the alignments of the longest and shortest edges. One simple Hamiltonian assigns energies to nearest-neighbor pairs proportionally to their projected area of overlap, thereby accounting for van der Waals attraction:

$$\begin{aligned}
&J(Z\bar{X},Z\bar{X})=-(ab+bc+ca)/3\ ,\\
&J(Z\bar{X},Y\bar{X})=-(b^2+2bc)/3\ ,\\
&J(Z\bar{X},Y\bar{Z})=J(Z\bar{X},X\bar{Z})=J(Z\bar{X},X\bar{Y})\\
&\qquad=-(2bc+c^2)/3\ ,\\
&J(Z\bar{X},Z\bar{Y})=-(2ac+c^2)/3\ .
\end{aligned} \quad (7)$$

As above, the pair interactions have been averaged over the relative positions of the two molecules. It can be verified that the energies given by Eqs. (7) satisfy[20] Eq. (5), so that the model maps onto the paired six-state clock model, namely onto the 6×6 block of the preceding treatment. The Migdal-Kadanoff renormalization-group pro-

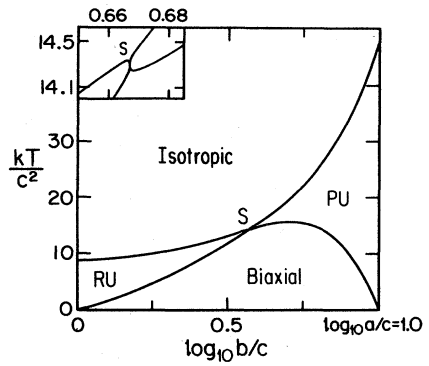

FIG. 4. Calculated phase diagram for a one-component system of biaxial molecules, with edge lengths $a>b>c$. The case $a/c=10$ is exhibited for varying b/c. The ordered phases are characterized by the alignment of either the long axes (RU), or the short axes (PU), or both (Biaxial).

cedure can again be applied. At this point, it would be appropriate to include effective vacancy fluctuations. We have not done so, and therefore obtain the possible second-order transitions. These are exhibited in Fig. 4, in the space of temperature and aspect ratio. In this system, either the long axes (RU), or the short axes (PU), or both axes (Biaxial) of the molecules order at low temperatures.

ACKNOWLEDGMENTS

This work has been supported by the National Science Foundation under Grants Nos. DMR81-19295 and CHE81-16613. The supports of a Fannie and John Hertz Fellowship for R.G.C. and an Alfred P. Sloan Fellowship for A.N.B. are also acknowledged.

*Present address: Schlumberger-Doll Research Center, Old Quarry Road, Ridgefield, Connecticut 06877.

†Present address: Department of Chemistry, University of California, Los Angeles, California 90024.

[1]M. J. Freiser, Phys. Rev. Lett. **24**, 1041 (1970); C.-S. Shih and R. Alben, J. Chem. Phys. **57**, 3055 (1972); R. Alben, Phys. Rev. Lett. **30**, 778 (1973); J. Chem. Phys. **59**, 4299 (1973); J. P. Straley, Phys. Rev. A **10**, 1881 (1974).

[2]More recent theoretical papers include W. M. Gelbart, J. Phys. Chem. **86**, 4298 (1982); Y. Rabin, W. E. McMullen, and W. M. Gelbart, Mol. Cryst. Liq. Cryst. **89**, 67 (1982).

[3]For the molecular-field treatment of the present model, see Z.-Y. Chen and J. M. Deutch, J. Chem. Phys. **80**, 2151 (1984).

[4]D. W. Allender and M. A. Lee (unpublished).

[5]L. J. Yu and A. Saupe, Phys. Rev. Lett. **45**, 1000 (1980); A. Saupe, P. Boonbrahm, and L. J. Yu, J. Chem. Phys. **80**, 7 (1983); R. Bartolino, T. Chiaranza, M. Meuti, and R. Compagnoni, Phys. Rev. A **26**, 116 (1982).

[6]R. Zwanzig, J. Chem. Phys. **39**, 1714 (1963).

[7]A. N. Berker, S. Ostlund, and F. A. Putnam, Phys. Rev. B **17**, 3650 (1978).

[8]R. G. Caflisch and A. N. Berker, Phys. Rev. B **29**, 1279 (1984).

[9]A. A. Migdal, Zh. Eksp. Teor. Fiz. **69**, 1457 (1975) [Sov. Phys.—JETP **42**, 743 (1976)]; L. P. Kadanoff, Ann. Phys. (N.Y.) **100**, 359 (1976); Rev. Mod. Phys. **49**, 267 (1977).

[10]B. Nienhuis, A. N. Berker, E. K. Riedel, and M. Schick, Phys. Rev. Lett. **43**, 737 (1979); A. N. Berker and D. Andelman, J. Appl. Phys. **53**, 7923 (1982).

[11]J. M. Kosterlitz and D. J. Thouless, J. Phys. C **6**, 1181 (1973); J. M. Kosterlitz, *ibid.* **7**, 1046 (1974).

[12]J. V. José, L. P. Kadanoff, S. Kirkpatrick, and D. R. Nelson, Phys. Rev. B **16**, 1217 (1977).

[13]Next-nearest-neighbor (diagonal) molecular interactions, added to the starting Hamiltonian of Eq. (1), could be easily treated in the present calculation. These interactions could in fact be used to enhance the similarity of the model to actual liquid crystal systems, which are close packed and therefore more coordinated than the cubic lattice. This inclusion would further stabilize the ordered phases, but is not expected to change qualitatively the results.

[14]R. B. Potts, Proc. Cambridge Philos. Soc. **48**, 106 (1952).

[15]A. N. Berker and L. P. Kadanoff, J. Phys. A **13**, L259 (1980).

[16]A. N. Berker and M. Wortis, Phys. Rev. B **14**, 4946 (1976).

[17]A. N. Berker, D. Andelman, and A. Aharony, J. Phys. A **13**, L413 (1980); D. Andelman and A. N. Berker, *ibid.* **14**, L91 (1981).

[18]J. S. Walker and C. A. Vause, Phys. Lett. A **79**, 421 (1980); R. G. Caflisch and J. S. Walker, Phys. Rev. B **28**, 2535 (1983).

[19]A. N. Berker (unpublished).

[20]In Sec. V the last relation of Eq. (5) is satisfied as an equality only at the initial points of renormalization-group trajectories.